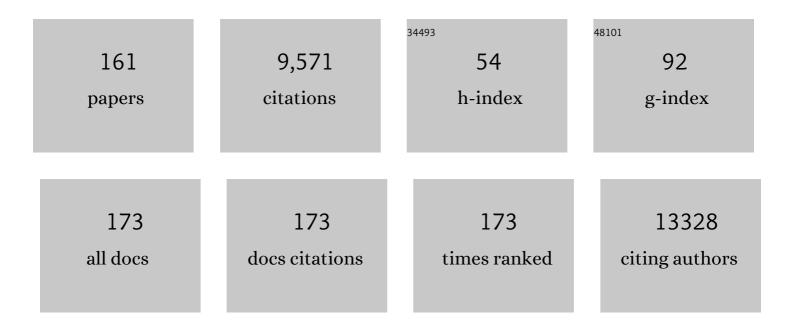
Henry Rusinek

List of Publications by Year in descending order

Source: https://exaly.com/author-pdf/495518/publications.pdf Version: 2024-02-01



#	Article	IF	CITATIONS
1	Image Segmentation and Nonuniformity Correction Methods. , 2022, , 31-43.		1
2	Repeatability, robustness, and reproducibility of texture features on 3ÂTesla liver MRI. Clinical Imaging, 2022, 83, 177-183.	0.8	4
3	Decreased CSF clearance and increased brain amyloid in Alzheimer's disease. Fluids and Barriers of the CNS, 2022, 19, 21.	2.4	41
4	Deep Learning Achieves Neuroradiologist-Level Performance in Detecting Hydrocephalus Requiring Treatment. Journal of Digital Imaging, 2022, 35, 1662-1672.	1.6	1
5	Bilateral Distance Partition of Periventricular and Deep White Matter Hyperintensities: Performance of the Method in the Aging Brain. Academic Radiology, 2021, 28, 1699-1708.	1.3	12
6	Visceral adipose tissue in patients with COVID-19: risk stratification for severity. Abdominal Radiology, 2021, 46, 818-825.	1.0	41
7	Preliminary Findings Associate Hippocampal ¹ H-MR Spectroscopic Metabolite Concentrations with Psychotic and Manic Symptoms in Patients with Schizophrenia. American Journal of Neuroradiology, 2021, 42, 88-93.	1.2	7
8	Quantitative imaging features predict spinal tap response in normal pressure hydrocephalus. Neuroradiology, 2021, , 1.	1.1	3
9	Assessment of Renal Cell Carcinoma by Texture Analysis in Clinical Practice: A Six-Site, Six-Platform Analysis of Reliability. American Journal of Roentgenology, 2021, 217, 1132-1140.	1.0	10
10	Tauâ€Atrophy Variability Reveals Phenotypic Heterogeneity in Alzheimer's Disease. Annals of Neurology, 2021, 90, 751-762.	2.8	19
11	Kidney tumor diffusion-weighted magnetic resonance imaging derived ADC histogram parameters combined with patient characteristics and tumor volume to discriminate oncocytoma from renal cell carcinoma. European Journal of Radiology, 2021, 145, 110013.	1.2	5
12	Peak ependymal cell stretch overlaps with the onset locations of periventricular white matter lesions. Scientific Reports, 2021, 11, 21956.	1.6	6
13	Association of body composition parameters measured on CT with risk of hospitalization in patients with Covid-19. European Journal of Radiology, 2021, 145, 110031.	1.2	11
14	The Brain-Nose Interface: A Potential Cerebrospinal Fluid Clearance Site in Humans. Frontiers in Physiology, 2021, 12, 769948.	1.3	15
15	Effects of blood pressure on white matter lesions and brain volumes in hypertensive and normotensive subjects Alzheimer's and Dementia, 2021, 17 Suppl 3, e053826.	0.4	0
16	Standardized Brain MRI Acquisition Protocols Improve Statistical Power in Multicenter Quantitative Morphometry Studies. Journal of Neuroimaging, 2020, 30, 126-133.	1.0	8
17	Assessment of metastatic lymph nodes in head and neck squamous cell carcinomas using simultaneous 18F-FDG-PET and MRI. Scientific Reports, 2020, 10, 20764.	1.6	16
18	PET imaging of net availability in humans using [11 C]MRB: Age, gender and ethnicity effects. Alzheimer's and Dementia, 2020, 16, e041956.	0.4	0

#	Article	IF	CITATIONS
19	Neuroimaging of amyloid pathology in a nonâ€human primate model of sporadic CAA. Alzheimer's and Dementia, 2020, 16, e045327.	0.4	0
20	Precisely-Measured Hydration Status Correlates with Hippocampal Volume in Healthy Older Adults. American Journal of Geriatric Psychiatry, 2019, 27, 653-654.	0.6	4
21	Different Relationship Between Systolic Blood Pressure and Cerebral Perfusion in Subjects With and Without Hypertension. Hypertension, 2019, 73, 197-205.	1.3	39
22	Prostate cancer heterogeneity: texture analysis score based on multiple magnetic resonance imaging sequences for detection, stratification and selection of lesions at time of biopsy. BJU International, 2019, 124, 76-86.	1.3	18
23	Basal forebrain septal nuclei are enlarged in healthy subjects prior to the development of Alzheimer's disease. Neurobiology of Aging, 2018, 65, 201-205.	1.5	25
24	REnal Flow and Microstructure AnisotroPy (REFMAP) MRI in Normal and Peritumoral Renal Tissue. Journal of Magnetic Resonance Imaging, 2018, 48, 188-197.	1.9	11
25	Reply:. American Journal of Neuroradiology, 2018, 39, E7-E7.	1.2	0
26	Quantitative evaluation of tau PET tracers 18F-THK5351 and 18F-AV-1451 in Alzheimer's disease with standardized uptake value peak-alignment (SUVP) normalization. European Journal of Nuclear Medicine and Molecular Imaging, 2018, 45, 1596-1604.	3.3	15
27	Comparison between qualitative and quantitative assessment of background parenchymal enhancement on breast MRI. Journal of Magnetic Resonance Imaging, 2018, 47, 1685-1691.	1.9	12
28	P2â€074: IMPAIRED CSF CLEARANCE AND BRAIN AMYLOID IN ALZHEIMER'S DISEASE: A MULTIâ€TRACER PET STU Alzheimer's and Dementia, 2018, 14, P695.	DY. 0.4	0
29	Accuracy and precision of quantitative DCE-MRI parameters: How should one estimate contrast concentration?. Magnetic Resonance Imaging, 2018, 52, 16-23.	1.0	22
30	The nonlinear relationship between cerebrospinal fluid Aβ42 and tau in preclinical Alzheimer's disease. PLoS ONE, 2018, 13, e0191240.	1.1	41
31	Clinical applicability and relevance of fibroglandular tissue segmentation on routine T1 weighted breast MRI. Clinical Imaging, 2017, 42, 119-125.	0.8	5
32	Diagnosis of Normal-Pressure Hydrocephalus: Use of Traditional Measures in the Era of Volumetric MR Imaging. Radiology, 2017, 285, 197-205.	3.6	85
33	Lumbar Puncture Test in Normal Pressure Hydrocephalus: Does the Volume of CSF Removed Affect the Response to Tap?. American Journal of Neuroradiology, 2017, 38, 1456-1460.	1.2	17
34	Proton MR spectroscopy of lesion evolution in multiple sclerosis: Steadyâ€state metabolism and its relationship to conventional imaging. Human Brain Mapping, 2017, 38, 4047-4063.	1.9	18
35	Insulin resistance among obese middle-aged is associated with decreased cerebrovascular reactivity. Neurology, 2017, 89, 249-255.	1.5	24
36	Cerebrospinal Fluid Clearance in Alzheimer Disease Measured with Dynamic PET. Journal of Nuclear Medicine, 2017, 58, 1471-1476.	2.8	161

#	Article	IF	CITATIONS
37	Lepidic Predominant Pulmonary Lesions (LPL). Academic Radiology, 2017, 24, 1604-1611.	1.3	12
38	3D Registration of mpMRI for Assessment of Prostate Cancer Focal Therapy. Academic Radiology, 2017, 24, 1544-1555.	1.3	7
39	Likert score 3 prostate lesions: Association between wholeâ€lesion ADC metrics and pathologic findings at MRI/ultrasound fusion targeted biopsy. Journal of Magnetic Resonance Imaging, 2016, 43, 325-332.	1.9	25
40	Assessment of renal function using intravoxel incoherent motion diffusionâ€weighted imaging and dynamic contrastâ€enhanced MRI. Journal of Magnetic Resonance Imaging, 2016, 44, 317-326.	1.9	37
41	Accelerated Brain Atrophy on Serial Computed Tomography. Journal of Computer Assisted Tomography, 2016, 40, 827-832.	0.5	17
42	Effects of vascular risk factors, statins, and antihypertensive drugs on PiB deposition in cognitively normal subjects. Alzheimer's and Dementia: Diagnosis, Assessment and Disease Monitoring, 2016, 2, 95-104.	1.2	24
43	Lung Adenocarcinoma: Correlation of Quantitative CT Findings with Pathologic Findings. Radiology, 2016, 280, 931-939.	3.6	74
44	Use of MRI in Differentiation of Papillary Renal Cell Carcinoma Subtypes: Qualitative and Quantitative Analysis. American Journal of Roentgenology, 2016, 206, 566-572.	1.0	40
45	A semi-automated "blanket―method for renal segmentation from non-contrast T1-weighted MR images. Magnetic Resonance Materials in Physics, Biology, and Medicine, 2016, 29, 197-206.	1.1	8
46	Wholeâ€lesion apparent diffusion coefficient metrics as a marker of percentage Gleason 4 component within Gleason 7 prostate cancer at radical prostatectomy. Journal of Magnetic Resonance Imaging, 2015, 41, 708-714.	1.9	71
47	Combined intravoxel incoherent motion and diffusion tensor imaging of renal diffusion and flow anisotropy. Magnetic Resonance in Medicine, 2015, 73, 1526-1532.	1.9	85
48	Cortical Laminar Binding of PET Amyloid and Tau Tracers in Alzheimer Disease. Journal of Nuclear Medicine, 2015, 56, 270-273.	2.8	22
49	High Spatiotemporal Resolution Dynamic Contrast-Enhanced MR Enterography in Crohn Disease Terminal Ileitis Using Continuous Golden-Angle Radial Sampling, Compressed Sensing, and Parallel Imaging. American Journal of Roentgenology, 2015, 204, W663-W669.	1.0	19
50	Cerebral Perfusion in Insulin Resistance and Type 2 Diabetes. Journal of Cerebral Blood Flow and Metabolism, 2015, 35, 95-102.	2.4	58
51	Calculation of brain atrophy using computed tomography and a new atrophy measurement tool. Proceedings of SPIE, 2015, , .	0.8	Ο
52	P4-253: Effects of metabolic syndrome, antihypertensive medications, and statins on PiB deposition in cognitively normal subjects. , 2015, 11, P878-P878.		0
53	P4-255: Normotensive elderly with white matter lesions: A group at risk for Alzheimer's disease. , 2015, 11, P879-P879.		0
54	Detection of third and sixth cranial nerve palsies with a novel method for eye tracking while watching a short film clip. Journal of Neurosurgery, 2015, 122, 707-720.	0.9	24

#	Article	IF	CITATIONS
55	Measurement reproducibility of magnetic resonance imaging-based finite element analysis of proximal femur microarchitecture for in vivo assessment of bone strength. Magnetic Resonance Materials in Physics, Biology, and Medicine, 2015, 28, 407-412.	1.1	15
56	Image Guided Focal Therapy for Magnetic Resonance Imaging Visible Prostate Cancer: Defining a 3-Dimensional Treatment Margin Based on Magnetic Resonance Imaging Histology Co-Registration Analysis. Journal of Urology, 2015, 194, 364-370.	0.2	146
57	Clearance systems in the brain—implications for Alzheimer disease. Nature Reviews Neurology, 2015, 11, 457-470.	4.9	1,127
58	Estimating Liver Perfusion From Free–Breathing Continuously Acquired Dynamic Gadolinium-Ethoxybenzyl-Diethylenetriamine Pentaacetic Acid–Enhanced Acquisition With Compressed Sensing Reconstruction. Investigative Radiology, 2015, 50, 88-94.	3.5	49
59	Prostate Cancer: Utility of Whole-Lesion Apparent Diffusion Coefficient Metrics for Prediction of Biochemical Recurrence After Radical Prostatectomy. American Journal of Roentgenology, 2015, 205, 1208-1214.	1.0	42
60	Reduced retention of Pittsburgh compound B in white matter lesions. European Journal of Nuclear Medicine and Molecular Imaging, 2015, 42, 97-102.	3.3	26
61	Periodontal disease associates with higher brain amyloid load in normal elderly. Neurobiology of Aging, 2015, 36, 627-633.	1.5	198
62	Whole-lesion diffusion metrics for assessment of bladder cancer aggressiveness. Abdominal Imaging, 2015, 40, 327-332.	2.0	31
63	Precision of volumetric assessment of proximal femur microarchitecture from high-resolution 3T MRI. International Journal of Computer Assisted Radiology and Surgery, 2015, 10, 35-43.	1.7	8
64	Prostate tumour volumes: evaluation of the agreement between magnetic resonance imaging and histology using novel coâ€registration software. BJU International, 2014, 114, E105-E112.	1.3	74
65	DCEâ€MRI of the liver: Effect of linear and nonlinear conversions on hepatic perfusion quantification and reproducibility. Journal of Magnetic Resonance Imaging, 2014, 40, 90-98.	1.9	63
66	Differentiating shunt-responsive normal pressure hydrocephalus from Alzheimer disease and normal aging: pilot study using automated MRI brain tissue segmentation. Journal of Neurology, 2014, 261, 1994-2002.	1.8	34
67	Comparison of human septal nuclei MRI measurements using automated segmentation and a new manual protocol based on histology. NeuroImage, 2014, 97, 245-251.	2.1	25
68	Blood pressure decrease correlates with tau pathology and memory decline in hypertensive elderly. Neurobiology of Aging, 2014, 35, 64-71.	1.5	66
69	New magnetic resonance imaging methods in nephrology. Kidney International, 2014, 85, 768-778.	2.6	84
70	Cerebral damage in obesity-associated metabolic syndrome. Nature Reviews Endocrinology, 2014, 10, 642-644.	4.3	13
71	Global N-Acetylaspartate in Normal Subjects, Mild Cognitive Impairment and Alzheimer's Disease Patients. Journal of Alzheimer's Disease, 2014, 43, 939-947.	1.2	27
72	Dynamic Contrast-Enhanced MR Renography for Renal Function Evaluation in Ureteropelvic Junction Obstruction: Feasibility Study. American Journal of Roentgenology, 2014, 202, 778-783.	1.0	16

#	Article	IF	CITATIONS
73	DCE-MRI of the Liver: Reconstruction of the Arterial Input Function Using a Low Dose Pre-Bolus Contrast Injection. PLoS ONE, 2014, 9, e115667.	1.1	14
74	Hepatocellular Carcinoma: Perfusion Quantification With Dynamic Contrast-Enhanced MRI. American Journal of Roentgenology, 2013, 201, 795-800.	1.0	81
75	Global gray and white matter metabolic changes after simian immunodeficiency virus infection in CD8â€depleted rhesus macaques: proton MRS imaging at 3 T. NMR in Biomedicine, 2013, 26, 480-488.	1.6	5
76	Characterization of malignancy of adnexal lesions using ADC entropy: Comparison with mean ADC and qualitative DWI assessment. Journal of Magnetic Resonance Imaging, 2013, 37, 164-171.	1.9	57
77	Comparison of 3â€point dixon imaging and fuzzy Câ€means clustering methods for breast density measurement. Journal of Magnetic Resonance Imaging, 2013, 38, 474-481.	1.9	28
78	Magnetic Resonance Imaging (MRI) of hormone-induced breast changes in young premenopausal women. Magnetic Resonance Imaging, 2013, 31, 1-9.	1.0	27
79	The Self-Overlap Method for Assessment of Lung Nodule Morphology in Chest CT. Journal of Digital Imaging, 2013, 26, 239-247.	1.6	6
80	Longitudinal quantitative analysis of the tuber-to-brain proportion in patients with tuberous sclerosis. Journal of Neurosurgery: Pediatrics, 2013, 12, 71-76.	0.8	4
81	Functional MRI of the kidneys. Journal of Magnetic Resonance Imaging, 2013, 37, 282-293.	1.9	72
82	Cerebrovascular Reactivity to Carbon Dioxide in Alzheimer's Disease. Journal of Alzheimer's Disease, 2013, 35, 427-440.	1.2	106
83	Renal Blood Oxygenation Level–Dependent Imaging. Investigative Radiology, 2013, 48, 501-508.	3.5	18
84	Pulmonary Nodules: Growth Rate Assessment in Patients by Using Serial CT and Three-dimensional Volumetry. Radiology, 2012, 262, 662-671.	3.6	69
85	Intravoxel Incoherent Motion and Diffusion-Tensor Imaging in Renal Tissue under Hydration and Furosemide Flow Challenges. Radiology, 2012, 263, 758-769.	3.6	185
86	Association of common genetic variants in GPCPD1 with scaling of visual cortical surface area in humans. Proceedings of the National Academy of Sciences of the United States of America, 2012, 109, 3985-3990.	3.3	50
87	Cerebral atrophy is associated with development of chronic subdural haematoma. Brain Injury, 2012, 26, 1731-1736.	0.6	73
88	Diffusion-Weighted Intravoxel Incoherent Motion Imaging of Renal Tumors With Histopathologic Correlation. Investigative Radiology, 2012, 47, 688-696.	3.5	100
89	The ADNI Publication Policy: Commensurate recognition of critical contributors who are not authors. NeuroImage, 2012, 59, 4196-4200.	2.1	5
90	Characterizing Brain Oxygen Metabolism in Patients with Multiple Sclerosis with <i>T2</i> -Relaxation-Under-Spin-Tagging MRI. Journal of Cerebral Blood Flow and Metabolism, 2012, 32, 403-412.	2.4	92

#	Article	IF	CITATIONS
91	Optimization of <i>b</i> â€value sampling for diffusionâ€weighted imaging of the kidney. Magnetic Resonance in Medicine, 2012, 67, 89-97.	1.9	98
92	Framingham Cardiovascular Risk Profile Correlates with Impaired Hippocampal and Cortical Vasoreactivity to Hypercapnia. Journal of Cerebral Blood Flow and Metabolism, 2011, 31, 671-679.	2.4	59
93	Hippocampal blood flow in normal aging measured with arterial spin labeling at 3T. Magnetic Resonance in Medicine, 2011, 65, 128-137.	1.9	26
94	A <i>B</i> ₁ â€insensitive high resolution 2D <i>T</i> ₁ mapping pulse sequence for dGEMRIC of the HIP at 3 Tesla. Magnetic Resonance in Medicine, 2011, 66, 348-355.	1.9	13
95	Kidney Function: Glomerular Filtration Rate Measurement with MR Renography in Patients with Cirrhosis. Radiology, 2011, 259, 462-470.	3.6	55
96	Quantitative Evaluation of Acute Renal Transplant Dysfunction with Low-Dose Three-dimensional MR Renography. Radiology, 2011, 260, 781-789.	3.6	35
97	An automated three-dimensional plus time registration framework for dynamic MR renography. Journal of Visual Communication and Image Representation, 2010, 21, 1-8.	1.7	9
98	Variability of Renal Apparent Diffusion Coefficients: Limitations of the Monoexponential Model for Diffusion Quantification. Radiology, 2010, 254, 783-792.	3.6	155
99	99mTc Hexamethyl-Propylene-Aminoxime Single-Photon Emission Computed Tomography Prediction of Conversion From Mild Cognitive Impairment to Alzheimer Disease. American Journal of Geriatric Psychiatry, 2010, 18, 959-972.	0.6	28
100	Magnetic Resonance Imaging Improves Cerebrospinal Fluid Biomarkers in the Early Detection of Alzheimer's Disease. Journal of Alzheimer's Disease, 2009, 16, 351-362.	1.2	60
101	Three-dimensional Electrocardiographically Gated Variable Flip Angle FSE Imaging for MR Angiography of the Hands at 3.0 T: Initial Experience. Radiology, 2009, 252, 874-881.	3.6	25
102	Angiotensin-converting enzyme inhibitor-enhanced MR renography: repeated measures of GFR and RPF in hypertensive patients. American Journal of Physiology - Renal Physiology, 2009, 296, F884-F891.	1.3	13
103	Estimates of glomerular filtration rate from MR renography and tracer kinetic models. Journal of Magnetic Resonance Imaging, 2009, 29, 371-382.	1.9	77
104	Use of cardiac output to improve measurement of input function in quantitative dynamic contrastâ€enhanced MRI. Journal of Magnetic Resonance Imaging, 2009, 30, 656-665.	1.9	32
105	Optimal <i>k</i> â€space sampling for dynamic contrastâ€enhanced MRI with an application to MR renography. Magnetic Resonance in Medicine, 2009, 61, 1242-1248.	1.9	126
106	Dynamic Contrast-Enhanced MR Imaging of the Liver: Current Status and Future Directions. Magnetic Resonance Imaging Clinics of North America, 2009, 17, 339-349.	0.6	59
107	Fully automatic segmentation of the brain from T1â€weighted MRI using <i>Bridge Burner</i> algorithm. Journal of Magnetic Resonance Imaging, 2008, 27, 1235-1241.	1.9	74
108	Functional assessment of the kidney from magnetic resonance and computed tomography renography: Impulse retention approach to a multicompartment model. Magnetic Resonance in Medicine, 2008, 59, 278-288.	1.9	65

#	Article	IF	CITATIONS
109	Hippocampal hypometabolism predicts cognitive decline from normal aging. Neurobiology of Aging, 2008, 29, 676-692.	1.5	292
110	Global average gray and white matter N-acetylaspartate concentration in the human brain. NeuroImage, 2008, 41, 270-276.	2.1	35
111	Assessment of Renal Function with Dynamic Contrast-Enhanced MR Imaging. Magnetic Resonance Imaging Clinics of North America, 2008, 16, 597-611.	0.6	63
112	Segmentation of 4D MR renography images using temporal dynamics in a level set framework. , 2008, , .		7
113	Advanced Liver Fibrosis: Diagnosis with 3D Whole-Liver Perfusion MR Imaging—Initial Experience. Radiology, 2008, 246, 926-934.	3.6	216
114	Renal function measurements from MR renography and a simplified multicompartmental model. American Journal of Physiology - Renal Physiology, 2007, 292, F1548-F1559.	1.3	130
115	Quantitative determination of Gd-DTPA concentration inT1-weighted MR renography studies. Magnetic Resonance in Medicine, 2007, 57, 1012-1018.	1.9	65
116	Performance of an automated segmentation algorithm for 3D MR renography. Magnetic Resonance in Medicine, 2007, 57, 1159-1167.	1.9	71
117	Benefit of CT venography for the diagnosis of thromboembolic disease. Clinical Imaging, 2007, 31, 253-258.	0.8	18
118	Early detection of Alzheimer's disease using neuroimaging. Experimental Gerontology, 2007, 42, 129-138.	1.2	140
119	Effect of Blood Vessels on Measurement of Nodule Volume in a Chest Phantom. Radiology, 2006, 239, 79-85.	3.6	23
120	Dose-related Nephrotoxicity. Radiology, 2006, 240, 614-614.	3.6	12
121	Clinical significance of dilated Virchow-Robin spaces in mild traumatic brain injury. Brain Injury, 2006, 20, 15-21.	0.6	29
122	Four Dimensional MR Image Analysis of Dynamic Renography. Annual International Conference of the IEEE Engineering in Medicine and Biology Society, 2006, , .	0.5	0
123	Appendicitis in Children: Low-Dose CT with a Phantom-based Simulation Technique—Initial Observations. Radiology, 2005, 237, 641-646.	3.6	39
124	Perfusion Imaging of the Liver: Current Challenges and Future Goals. Radiology, 2005, 234, 661-673.	3.6	263
125	Effect of CT Image Compression on Computer-assisted Lung Nodule Volume Measurement. Radiology, 2005, 237, 83-88.	3.6	29
126	The Role of Quantitative Structural Imaging in the Early Diagnosis of Alzheimer's DiseaseQ4. Neuroimaging Clinics of North America, 2005, 15, 803-826.	0.5	39

#	Article	IF	CITATIONS
127	Assessing global invasion of newly diagnosed glial tumors with whole-brain proton MR spectroscopy. American Journal of Neuroradiology, 2005, 26, 2170-7.	1.2	31
128	Brain compression without global neuronal loss in meningiomas: whole-brain proton MR spectroscopy report of 2 cases. American Journal of Neuroradiology, 2005, 26, 2178-82.	1.2	6
129	Dilated perivascular spaces: hallmarks of mild traumatic brain injury. American Journal of Neuroradiology, 2005, 26, 719-24.	1.2	70
130	Assessment of Vasculature Using Combined MRI and MR Angiography. American Journal of Roentgenology, 2004, 182, 861-866.	1.0	20
131	Magnetic resonance and PET studies in the early diagnosis of Alzheimer's disease. Expert Review of Neurotherapeutics, 2004, 4, 831-849.	1.4	41
132	Functional renal MR imaging. Magnetic Resonance Imaging Clinics of North America, 2004, 12, 469-486.	0.6	55
133	Renal magnetic resonance imaging. Current Opinion in Nephrology and Hypertension, 2004, 13, 667-673.	1.0	17
134	MR imaging of renal function. Radiologic Clinics of North America, 2003, 41, 1001-1017.	0.9	41
135	Small Pulmonary Nodules: Volume Measurement at Chest CT—Phantom Study. Radiology, 2003, 228, 864-870.	3.6	190
136	Dynamic Three-dimensional MR Renography for the Measurement of Single Kidney Function: Initial Experience. Radiology, 2003, 227, 289-294.	3.6	121
137	Regional Brain Atrophy Rate Predicts Future Cognitive Decline: 6-year Longitudinal MR Imaging Study of Normal Aging. Radiology, 2003, 229, 691-696.	3.6	253
138	Wavelet Compression of Low-Dose Chest CT Data: Effect on Lung Nodule Detection. Radiology, 2003, 228, 70-75.	3.6	60
139	CT Findings in Acute Gangrenous Cholecystitis. American Journal of Roentgenology, 2002, 178, 275-281.	1.0	182
140	Computed Tomography Diagnosis Utilizing Compressed Image Data: An ROC Analysis Using Acute Appendicitis as a Model. Journal of Digital Imaging, 2002, 15, 84-90.	1.6	14
141	Cognitive performance in schizophrenia: relationship to regional brain volumes and psychiatric symptoms. Psychiatry Research - Neuroimaging, 2002, 116, 1-23.	0.9	112
142	Hippocampal formation glucose metabolism and volume losses in MCI and AD. Neurobiology of Aging, 2001, 22, 529-539.	1.5	511
143	Segmentation of Dynamic N-D Data Sets via Graph Cuts Using Markov Models. Lecture Notes in Computer Science, 2001, , 1058-1066.	1.0	39
144	Optimal dose of Gd-DTPA in dynamic MR studies. Magnetic Resonance in Medicine, 2001, 46, 312-316.	1.9	51

#	Article	IF	CITATIONS
145	MR Renography with Low-Dose Gadopentetate Dimeglumine: Feasibility. Radiology, 2001, 221, 371-379.	3.6	64
146	Structural Magnetic Resonance Image Averaging in Schizophrenia. American Journal of Psychiatry, 1998, 155, 1064-1073.	4.0	72
147	Effect of a Haloperidol Challenge on Regional Brain Metabolism in Neuroleptic-Responsive and Nonresponsive Schizophrenic Patients. American Journal of Psychiatry, 1998, 155, 337-343.	4.0	63
148	Contribution of Structural Neuroimaging to the Early Diagnosis of Alzheimer's Disease. International Psychogeriatrics, 1997, 9, 183-190.	0.6	82
149	Time-dependent effects of a haloperidol challenge on energy metabolism in the normal human brain. Psychiatry Research, 1996, 60, 91-99.	1.7	14
150	Design of gradient coils for permanent magnets. Journal of Magnetic Resonance Imaging, 1996, 6, 239-243.	1.9	2
151	Age-related changes in brain: I. Magnetic resonance imaging measures of temporal lobe volumes in normal subjects. Psychiatric Quarterly, 1995, 66, 343-355.	1.1	38
152	Age-related changes in brain: II. Positron emission tomography of frontal and temporal lobe glucose metabolism in normal subjects. Psychiatric Quarterly, 1995, 66, 357-370.	1.1	72
153	Compensation of field distortion with ferromagnetic materials and permanent magnets. Journal of Applied Physics, 1994, 75, 6990-6992.	1.1	6
154	Long term study of random noise and signal uniformity in spin-echo brain imaging. Medical Physics, 1993, 20, 1071-1075.	1.6	1
155	Brain Tissue Volume Measurement from Magnetic Resonance Imaging A Phantom Study. Investigative Radiology, 1993, 28, 890-895.	3.5	28
156	Variables Affecting Pulmonary Nodule Detection with Computed Tomography. Journal of Thoracic Imaging, 1993, 8, 291-299.	0.8	60
157	Protruding aortic atheromas predict stroke in elderly patients undergoing cardiopulmonary bypass: Experience with intraoperative transesophageal echocardiography. Journal of the American College of Cardiology, 1992, 20, 70-77.	1.2	459
158	A comparison of two approaches to three-dimensional imaging of craniofacial anomalies. Journal of Digital Imaging, 1990, 3, 81-88.	1.6	7
159	Compensation of non-uniform magnetic properties of components of a yokeless permanent magnet. IEEE Transactions on Magnetics, 1989, 25, 3904-3906.	1.2	7
160	Interactive graphic editor for analysis and enhancement of medical images. Journal of Biomedical Informatics, 1989, 22, 328-338.	0.7	2
161	Neuroimaging of cognitive disorders: commentary. , 0, , 395-402.		0